Design and Control of a Multirotor for Application or Removal of Painting Systems

Luís Monteiro Casquinho Júdice Sousa
luis.judice@tecnico.ulisboa.pt

Instituto Superior Técnico, Universidade de Lisboa
Lisboa, Portugal

July 2017

Abstract

Recently, unmanned multirotors have been assuming an important role in the automation of numerous processes in different industries. The aim of this project is the design and control of an autonomous multirotor with the ability to perform the operations associated with aircraft painting or paint removal, under variable mass conditions. First, the concept is described, the platform is sized and its components are selected, based on the project requirements. The platform design allowed the identification of its structural properties, from which the multirotor has been modelled in MatLab/Simulink. The final model consists in a coaxial octorotor with variable mass and subject to changes in its centre of gravity and its inertia tensor. With the multirotor model defined, two adaptive controllers were developed to cope with the changes in mass and inertia properties of the octorotor, using a Linear Quadratic Regulator as the basis for stabilizing its attitude and position. The first controller makes use of an Extended Kalman Filter to estimate the mass of the system at each moment and correct the trim input accordingly. The second controller is based on the Model Reference Adaptive Control scheme using the Lyapunov method and is used to adapt the vertical dynamics of the octorotor. Finally, the performance of these controllers was analysed and compared.
Keywords: Multirotor, Application of Organic Coatings, Adaptive Control, Extended Kalman Filter, Model Reference Adaptive Control

1. Introduction

Multirotors are a type of Unmanned Aerial Vehicles (UAV) that are capable of vertical take-off and landing (VTOL). This kind of UAV is also characterized by the ability of hovering and low speed flight and has great maneuverability. Due to these characteristics, these aircrafts can be used in numerous applications in the military and civil domains, such as search and rescue missions, transportation of goods, and others. Hence, multirotors have been subject of great interest, not only from the scientific community but also from several industries. One of the most studied ideas has been the possibility of implementing unmanned multirotors for the automation of processes that involve high risk or cost.

In the aeronautical industry, one of the processes where automation would have a greater impact is the application and removal of organic coatings in aircrafts. Nowadays, the maintenance of the aircraft finishing system is a completely manual process, carried out by skilled labor. This is a time consuming process, developed in an hazardous environment. The automation of this process would be able to reduce its execution time and the amount of labor involved, which would lead to a reduction in costs, and environmental and health risks.

The search for automated solutions to carry out the application and removal of aircrafts finishing systems has been intensifying recently [1]. The aim of this project is to develop an autonomous multirotor platform that is able, to some extent, to perform these kind of functions. This is carried out, in a first stage, by designing the platform, through the selection of the necessary components. Then, a dynamic model of the multirotor is developed to study the implementation of control strategies that allow it to deal with the variable mass properties and off-centered center of gravity that arise from the task to be performed.

2. Platform Design

The platform was designed based on a set of requirements. Due to time restrictions, only the painting process was considered. Furthermore, there are several painting methods used in the industry, hence it was selected only one of them. The method chosen was the HVLP (High Volume Low Pressure)

spray painting, not only because it needs lighter and smaller equipment compared with the other methods, but also because it provides better finishing results [2].

The platform was then designed as an autonomous coaxial octorotor that would be able to carry all the equipment in flight. The coaxial configuration was chosen because it allows the installation of larger propellers.

2.1. Reference Mission

In order to limit the scope of the project, a reference mission was defined to determine the minimum operation time and the amount of coating material needed.

First, the area to be painted was defined as being half of the cargo compartment of a C-130 aircraft. According to [3], this area was determined to be $A_{ref} = 83.1m^2$. Thus, considering the specifications of spray painting technique recommended by several technical manuals such as [4] and [5], an estimate of the minimum operation time was determined as being $t_{op} \approx 10min$.

Knowing the area, the amount of coating material needed was determined, considering the application of an epoxy primer coating. Taking into account the allowable coat thickness range [2] and the concept of Practical Spreading Rate [6], the volume of primer needed was defined as $V_{primer} \approx 4.5L$. Considering the typical specific mass of this kind of coatings, this volume results in a mass of $m_{primer} \approx 6.3Kg$.

2.2. Spray Painting Equipment

To install an HVLP spray painting system on the octorotor, the necessary equipment is [2]: an HVLP turbine as the compressed air source, an HVLP spray gun and a pressure feed tank as the material container. In this project, since the aim is to have a completely autonomous platform, a power inverter is also needed to drive energy from a battery to the turbine.

The turbine, the spray gun and the power inverter were chosen as off-the-shelf components, based on a comparison between manufacturers. The criteria used was mainly the weight and dimensions of the components, and the ability to fulfill the task at hand. In turn, the pressure tanks available on the market did not meet the requirements imposed for maximum weight and dimensions. As such, this component was designed following the European Union's Pressure Equipment Directive (PED) [7]. In accordance with said directive, a $5L$ aluminum alloy coating material container was designed having a wall thickness of $5mm$. This tank has a total height of $23cm$, an external diameter of $26cm$, and its weight was estimated by SolidWorks® in approximately $5Kg$.

2.3. Off-the-Shelf Octorotor Components

After the definition of the concept, and knowing the weight of the painting equipment to be carried, it was possible to choose the octorotor components. The majority of these components is available on the market, so they were selected off-the-shelf. The selection process was carried out by comparing the alternatives available for each component, based on a set of criteria and the project requirements. The criteria followed were specific to each component and the details of the selection process are presented in the original thesis document. The components chosen for the octorotor were:

- 1 airframe GD-X8 1400 Super Frame with a distance between motors of $140cm$;
- 8 motors T-Motor U11 with the ability to produce $10Kg$ of maximum thrust each;
- 8 propellers T-Motor Carbon Fiber with $74cm$ in diameter;
- 8 Electronic Speed Controllers (ESC) EMAX BLHeli of $60A$;
- 5 batteries GensAce Tattu with a capacity of $30000mAh$ at $25C$ - 4 for the motors and 1 for the power inverter;
- 1 control unit PixHawk;
- 1 three-dimensional position sensor Pozyx with centimeter precision;
- 1 wireless communication system Digi® XBee;

2.4. Designed Octorotor Components

Even though the majority of the octorotor components was selected off-the-shelf, there are two components, related to the specificity of the project, which had to be designed. These components are a support structure where the painting equipment would be installed and an articulated arm to orient the spray gun with respect to the work surface. The two components were designed as being composed of a carbon fiber and epoxy resin composite material as it gives them a great mechanical strength combined with a low weight.

The support for the painting equipment consists of a structure with two levels: the HVLP turbine and the power inverter would be installed in the upper level, whereas the paint tank would go on the lower level. Having in consideration the dimensions and the weight of this equipment, each level consists of a square plate with sides having a length of $40cm$ and a thickness of $5mm$. This structure was modelled in SolidWorks® and its weight was estimated in $6Kg$. Figure 1 shows the representation of the structure in SolidWorks®.

Figure 1: Support structure

A finite element structural analysis was also carried out in ANSYS®, to ensure that the support structure would be able to cope with the all the loads that it will sustain. The details of this analysis are once again presented in the thesis document.

The articulated arm is used to hold and maneuver the spray gun, and is divided in three parts: a fixed base, the articulated extension and a fitting for the spray gun with a trigger actuator. In order to be able to hold the spray gun pointing forward or downward, the arm has a total length of $60cm$ and the moving part has a length of $33cm$. This component was also modelled in SolidWorks® and is shown in figure 2.

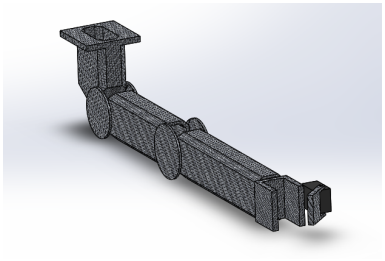

Figure 2: Articulated arm

This arm is only capable of moving in the vertical plane and its movement is controlled by two servo motors located in the second joint. The trigger actuator is also a servo motor. As such, the arm would have a total estimated weight, with the servos, of $3.1Kg$.

2.5. Final Platform

After the main components of this platform were chosen or designed, a coaxial octorotor was obtained with the ability for autonomous flight and to perform the task of application of organic coatings. In order to visualize the final platform, and to determine its mass and inertia properties, every component was modelled in SolidWorks® and assembled according to the concept.

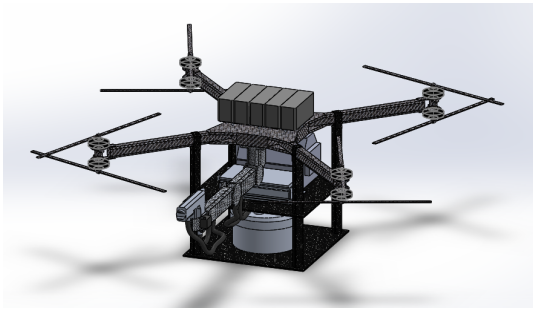

Figure 3: Final platform

As mentioned before, not only is this a heavy platform, but its total weight also varies throughout the operation due to the decrease in the amount of coating material present in the container. As such, this platform was modelled considering both extreme situations: pressure tank full (initial state, i) and empty (final state, f). The SolidWorks® model allowed the determination of its weight, the position of its center of gravity and its inertia tensor taken at that point, respectively, for both configurations:

$$m_i = 62.8Kg, \quad m_f = 56.5Kg \tag{1}$$

$$\begin{aligned} \boldsymbol{r_{Gi}} &= (0.008, 0, 0.144)[m], \\ \boldsymbol{r_{Gf}} &= (0.009, 0, 0.118)[m] \end{aligned} \tag{2}$$

$$\begin{aligned} \boldsymbol{J_{Gi}} &= \begin{bmatrix} 4.695 & -0.008 & -0.044 \\ -0.008 & 5.851 & 0.001 \\ -0.044 & 0.001 & 5.728 \end{bmatrix} [Kgm^2], \\ \boldsymbol{J_{Gf}} &= \begin{bmatrix} 4.209 & -0.008 & -0.03 \\ -0.008 & 5.369 & 0.001 \\ -0.03 & 0.001 & 5.693 \end{bmatrix} [Kgm^2] \end{aligned} \tag{3}$$

where m is the octorotor mass, $\boldsymbol{r_G}$ represents the position of its center of gravity and $\boldsymbol{J_G}$ is its inertia tensor taken at that point.

The motor/propeller configuration chosen has the ability to produce a maximum thrust of around $10Kg$ each. This results in a maximum total thrust of approximately $80Kg$ for the combined 8 rotors, which gives a thrust margin of around 30%.

2.6. Flight Time

The octorotor uses four batteries to supply energy to the motors. Its flight time was determined considering the batteries overall capacity and the motors total power consumption. The efficiency loss of the motors due to the coaxial configuration was also accounted for. Hence, it was determined that the octorotor has a flight time of approximately 15 minutes. It was concluded that the use of the coaxial configuration results in a reduction of approximately 12% in flight time.

3. Multirotor Modelling

In order to simulate the platform behaviour and to implement the control strategies to be studied, the system dynamics was modelled. In this project, the multirotor modelling was carried out in two steps. First, a conventional quadrotor was modelled, following the usual assumptions, mentioned in [8]. After making the necessary adjustments, the dynamic model of a coaxial octorotor with variable mass, off-centered center of gravity and non-diagonal inertia tensor was finally obtained. A simplified model, simulating only the vertical dynamics of the multirotor with variable mass, was also determined so that the adaptive control strategies could be easily tested and compared. Here, the final dynamic model of the octorotor and the simplified model are presented.

3.1. Coordinate Systems and Maneuverability

To describe the octorotor dynamics, two coordinate systems are defined: an earth fixed frame and a body fixed frame. The earth fixed reference frame is defined by $\Re_I = \{O_{NED}; X_I, Y_I, Z_I\}$ and is assumed to be inertial. Its origin is fixed on the ground and its axes point towards North, East and Down (X_I, Y_I and Z_I respectively). The body fixed frame, in turn, is a mobile frame defined by $\Re_B = \{O_B; x_B, y_B, z_B\}$ and its origin is coincident with the multirotor geometric center. Usually, this point coincides with the center of gravity of the body, but here this is not the case. Both coordinate systems are shown in figure 4 for the quadrotor case.

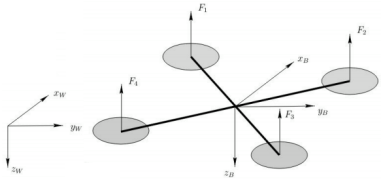

Figure 4: Coordinate systems used

The octorotor has six degrees of freedom that can be described by 12 states. The position of O_B relative to the fixed frame, $\boldsymbol{\xi} = [x\ y\ z]^T$, and the corresponding linear velocities expressed in the body frame, $\boldsymbol{V} = [u\ v\ w]^T$, describe the translational motion of the octorotor. Its attitude is described by the Euler angles, $\boldsymbol{\eta} = [\phi\ \theta\ \psi]^T$ (roll, pitch and yaw, respectively), and the angular velocities expressed in the body fixed frame are given by $\boldsymbol{\omega} = [p\ q\ r]^T$.

To convert any vector, described in the body frame, to the earth frame, a rotation matrix is needed. This matrix is the product of three other matrices ($\boldsymbol{R}(\psi)$, $\boldsymbol{R}(\theta)$ and $\boldsymbol{R}(\phi)$) and is given by [9]:

$$\boldsymbol{R} = \begin{bmatrix} c_\psi c_\theta & c_\psi s_\theta s_\phi - s_\psi c_\phi & c_\psi s_\theta c_\phi + s_\psi s_\phi \\ s_\psi c_\theta & s_\psi s_\theta s_\phi + c_\psi c_\phi & s_\psi s_\theta c_\phi - c_\psi s_\phi \\ -s_\theta & c_\theta s_\phi & c_\theta c_\phi \end{bmatrix} \quad (4)$$

with $c. = \cos(.)$ and $s. = \sin(.)$.

The octorotor is composed of four pairs of coaxial counter-rotating rotors (figure 5) and its attitude (roll, pitch and yaw motions) and altitude are controlled by changing the rotation speed of each one of them individually [9], [10].

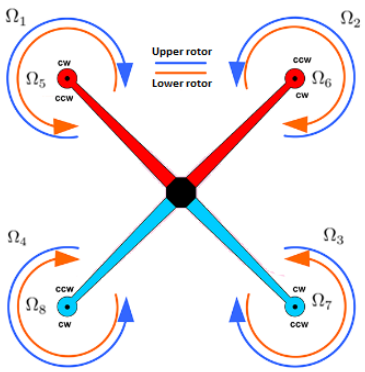

Figure 5: Numbering and rotation direction of the rotors

3.2. Kinematic Equations

The kinematic equations of the octorotor are given by:

$$\dot{\boldsymbol{\xi}} = \boldsymbol{RV} \quad (5)$$

$$\dot{\boldsymbol{\eta}} = \boldsymbol{S\omega} \quad (6)$$

Equation 5 defines the linear velocity of the octorotor in the inertial frame from its velocity expressed in the body fixed frame, where R comes from equation 4. In turn, equation 6 describes the relation between the derivatives of the Euler angles and the angular velocities expressed in the body fixed frame. Matrix S is defined as:

$$\boldsymbol{S} = \begin{bmatrix} 1 & s_\phi t_\theta & c_\phi t_\theta \\ 0 & c_\phi & -s_\phi \\ 0 & s_\phi / c_\theta & c_\phi / c_\theta \end{bmatrix} \quad (7)$$

with $t. = \tan(.)$.

3.3. System Dynamics

The dynamics of a multirotor are usually described using the Newton-Euler approach. In this work, since the center of gravity of the system is displaced from the origin of the body fixed frame, additional terms appear in the equations of motion. Therefore, the octorotor translational and rotational dynamics are respectively described by [11]:

$$\boldsymbol{F_p} + \boldsymbol{F_g} + \boldsymbol{F_a} = m\frac{\mathrm{d}\boldsymbol{V}}{\mathrm{d}t} + \boldsymbol{\omega} \times m\boldsymbol{V} + \\ + \frac{\mathrm{d}\boldsymbol{\omega}}{\mathrm{d}t} \times m\boldsymbol{r_G} + \boldsymbol{\omega} \times \boldsymbol{\omega} \times m\boldsymbol{r_G} \tag{8}$$

$$\boldsymbol{M_p} + \boldsymbol{M_g} + \boldsymbol{M_a} = \boldsymbol{J_{O_B}}\frac{\mathrm{d}\boldsymbol{\omega}}{\mathrm{d}t} + \boldsymbol{\omega} \times \boldsymbol{J_{O_B}}\boldsymbol{\omega} + \\ + m\boldsymbol{r_G} \times \frac{\mathrm{d}\boldsymbol{V}}{\mathrm{d}t} + m\boldsymbol{r_G} \times \boldsymbol{\omega} \times \boldsymbol{V} \tag{9}$$

In equation 8, force due to gravity is defined as $\boldsymbol{F_g} = m\boldsymbol{R}^T[0\ \ 0\ \ g]^T$, with $g = 9.81m/s^2$ and the aerodynamic force is given by $\boldsymbol{F_a} = -\boldsymbol{K_a}|\boldsymbol{V_a}|\boldsymbol{V_a}$ where $\boldsymbol{K_a}$ is the aerodynamic coefficients matrix and $\boldsymbol{V_a}$ is the air speed. The total thrust force, $\boldsymbol{F_p}$ represents the forces created by the propellers and is given by:

$$\boldsymbol{F_p} = [0\ \ 0\ \ -\sum_{i=1}^{8} T_i]^T \tag{10}$$

Equation 9 describes the rotational motion of the system, where $\boldsymbol{M_g} = \boldsymbol{r_G} \times \boldsymbol{F_g}$ and $\boldsymbol{M_a} = \boldsymbol{r_G} \times \boldsymbol{F_a}$. The thrust moment, $\boldsymbol{M_p}$ is defined as:

$$\boldsymbol{M_p} = \begin{bmatrix} \frac{\sqrt{2}}{2}b(T_1 - T_2 - T_3 + T_4 + T_5 - T_6 - T_7 + T_8) \\ \frac{\sqrt{2}}{2}b(T_1 + T_2 - T_3 - T_4 + T_5 + T_6 - T_7 - T_8) \\ -Q_1 + Q_2 - Q_3 + Q_4 + Q_5 - Q_6 + Q_7 - Q_8 \end{bmatrix} \tag{11}$$

The position of the center of gravity in the body frame changes, as stated previously, with the total mass of the octorotor. As such, it was assumed that the components of the vector $\boldsymbol{r_G}$ change linearly with the mass of the octorotor, taking into account the values obtained for the initial and final states (equations 1 and 2). Furthermore, as it can be seen in equation 3, the inertia tensor taken at the center of gravity also changes with the mass of the octorotor. This variation was also assumed linear. The matrix $\boldsymbol{J_{O_B}}$ represents the inertia tensor taken at O_B and is obtained from $\boldsymbol{J_G}$ applying the Huygens-Steiner theorem [12].

3.4. Actuators Dynamics

The actuation system of the octorotor is composed by the eight rotors, each of them composed by one motor and one propeller. The motors take as input the voltage from the batteries and convert it to angular velocity. In this work, the actual input for each motor is $\delta_i = \frac{V_{m_i}}{V_b}$, which is the voltage supplied to the motor, normalized by the total voltage of the batteries. The dynamics of the motors were then modelled as a second order system, with the usual parameters of brushless DC (Direct Current) motors [9].

On the other hand, propellers convert the angular velocity of the motors to a thrust force, T_i, and moment, Q_i that can be described by equations 12 and 13 [13].

$$T_i = C_T \rho A_h R_h^2 \Omega_i^2 \tag{12}$$

$$Q_i = C_Q \rho A_h R_h^3 \Omega_i^2 \tag{13}$$

where A_h represents the rotor disk area, R_h is the propeller radius, and C_T and C_Q represent its thrust and moment coefficients, respectively.

3.5. Simplified Model

A simplified model was developed in order to study the implementation of the adaptive control strategies and compare their performance when dealing with changes in the mass of the system. This model was derived considering a rigid body of variable mass m with its motion restricted to the vertical axis. The forces acting on the body are limited to the gravity force, in this case given by $F_g = -mg$ and a force U, that represents the total thrust of the system.

As it is the case for the octorotor, the mass of this system varies between two known values, $m_f \leq m \leq m_i$. In order to expedite the manipulation of the model when implementing the adaptive controllers, a new variable was introduced, defined by $\Theta = \frac{m_f}{m}$. Having that in consideration, the dynamics of the simplified model can be described as:

$$\dot{w}_s = -g + \frac{1}{m_f}\Theta U \tag{14}$$

where w_s is the body's linear vertical velocity.

3.6. Linearized Octorotor Model

The linearization of the octorotor model was carried out by implementing the first order Taylor series expansion to the dynamic equations of the system around an operating point. This operating point was considered as the hover situation.

The model was linearized considering the offset between the center of gravity and O_B, and with the non-diagonal inertia tensor, so that the adaptive controllers could be implemented.

Considering the state vector as $\boldsymbol{x} = [\boldsymbol{V}, \boldsymbol{\omega}, \boldsymbol{\xi}, \boldsymbol{\eta}]^T$ and the input vector as $\boldsymbol{u} = \boldsymbol{\Omega} = [\Omega_1, \Omega_2, \Omega_3, \Omega_4, \Omega_5, \Omega_6, \Omega_7, \Omega_8]^T$, the linearized system is defined as:

$$\dot{\boldsymbol{x}} = \boldsymbol{A_G}\boldsymbol{x} + \boldsymbol{B_G}\boldsymbol{u} \tag{15}$$

where matrices $\boldsymbol{A_G}$ and $\boldsymbol{B_G}$ are defined as the Jacobian of the nonlinear dynamics equations around the operating point.

4. LQR Controller

As a basis for the implementation of the adaptive control strategies on the octorotor model, a 12 states Linear Quadratic Regulator (LQR) controller was designed. This is an optimal controller that was used to close the loop, stabilizing the attitude of the octorotor and controlling its horizontal motion. First, the LQR was designed to control the 12 states of the system. After that, the adaptive controllers were implemented in the model as altitude control loops.

Considering the state-space system of the octorotor model described by equation 15, the LQR control problem consists in finding the optimal control action $\boldsymbol{u} = -\boldsymbol{K_{LQR}}\boldsymbol{x}$ that minimizes a cost function, representing the control signal energy, given by [14]:

$$J_{LQR} = \frac{1}{2}\int_0^\infty (\boldsymbol{x}^T\boldsymbol{Q_{LQR}}\boldsymbol{x} + \boldsymbol{u}^T\boldsymbol{R_{LQR}}\boldsymbol{u})dt \quad (16)$$

where $\boldsymbol{Q_{LQR}}$ and $\boldsymbol{R_{LQR}}$ are the positive-definite weighting matrices.

Hence, the gain matrix is defined as $\boldsymbol{K_{LQR}} = \boldsymbol{R_{LQR}}^{-1}\boldsymbol{B_G}^T\boldsymbol{P}$, with $\boldsymbol{P}$ being the solution of the algebraic Riccati equation [14]. Matrices $\boldsymbol{Q_{LQR}}$ and $\boldsymbol{R_{LQR}}$ are determined using the Bryson's method [10], followed by an iterative process to arrive to the desired results.

After the LQR gain matrix was determined, it was adjusted to account for the actuation dynamics and the result was applied to the pseudo-inverse of the allocation matrix [15], $\boldsymbol{M}^+$, in order to obtain the normalized voltage, δ_i, for each motor. For the coaxial octorotor, the allocation matrix, $\boldsymbol{M}$, is given by:

$$\boldsymbol{M} = \begin{bmatrix} 1 & 1 & 1 & 1 & 1 & 1 & 1 & 1 \\ 1 & -1 & -1 & 1 & 1 & -1 & -1 & 1 \\ 1 & 1 & -1 & -1 & 1 & 1 & -1 & -1 \\ -1 & 1 & -1 & 1 & -1 & 1 & -1 & 1 \end{bmatrix} \quad (17)$$

As such, an LQR controller was obtained to stabilize and control the 12 states of the octorotor model, described by:

$$\boldsymbol{\Delta} = \boldsymbol{\Delta}_0 - \boldsymbol{M}^+\frac{1}{G_a(0)}\boldsymbol{K_{LQR}}(\boldsymbol{x} - \boldsymbol{x}_0 - \boldsymbol{x}_{ref}) \quad (18)$$

where $\boldsymbol{\Delta}_0$ is the trim input vector, $\boldsymbol{x}_0$ is the trim state vector, $\boldsymbol{x}_{ref}$ is the reference input vector and $G_a(0)$ is the static gain of the actuation system.

5. Adaptive Control Strategies

In order to deal with the variable dynamics of the octorotor, two adaptive control approaches were conceived. The first strategy makes use of an Extended Kalman Filter (EKF) to estimate Θ at each moment and then uses that information to adapt the trim input accordingly. Alternatively, the second controller uses the Model Reference Adaptive Control (MRAC) scheme following the Lyapunov method to adapt the vertical dynamics of the system. These controllers were tested using the simplified model described earlier and were then applied to the octorotor model as an altitude control loop in the final controller.

5.1. State-Space Simplified Model

To implement the aforementioned controllers to the simplified model, it was necessary to write it in state-space formulation. Considering the state vector of this model as $\boldsymbol{x_s} = [w_s \;\; h_s]^T$ and the input as $u_s = U$, and choosing the operation point as the hover situation with mass m_f, the resulting system is given by:

$$\begin{bmatrix} \dot{w}_s \\ \dot{h}_s \end{bmatrix} = \begin{bmatrix} 0 & 0 \\ 1 & 0 \end{bmatrix}\begin{bmatrix} w_s \\ h_s \end{bmatrix} + \begin{bmatrix} \frac{1}{m_f} \\ 0 \end{bmatrix} u_s \quad (19)$$

where h_s denotes the altitude of the system.

5.2. EKF with Trim Input Adaptation

The EKF is a modification of the conventional Kalman Filter. While the Kalman Filter is an estimation method that allows for the estimation of the instantaneous state of a linear dynamic system affected by white noise, the EKF is applied in situations where the state dynamics or the observation dynamics of the system are nonlinear [16]. In this case, the system is linearized about the current estimates.

The simplified model, that corresponds to the vertical dynamics of the octorotor, has a nonlinear state dynamics, whereas its observation dynamics is considered to be linear. As such, the discrete model can be described by equation 20.

$$\boldsymbol{x}_{k+1} = f(\boldsymbol{x}_k, u_k) + \boldsymbol{v}_k, \quad \boldsymbol{y}_k = \boldsymbol{C}\boldsymbol{x}_k + \boldsymbol{n}_k \quad (20)$$

where $\boldsymbol{v}_k$ is the process noise with covariance $\boldsymbol{Q}_k$, $\boldsymbol{n}_k$ is the measurement noise with covariance $\boldsymbol{R}_k$ and $\boldsymbol{C}$ is the observation matrix. Since the aim is to estimate Θ to know the mass of the system at each moment, the state vector was modified to include this variable as $\boldsymbol{x}_k = [w_k \;\; h_k \;\; \Theta_k]^T$.

Initially, the EKF, through f, uses the current state estimate, $\hat{\boldsymbol{x}}_{k|k}$, to predict the future state, $\hat{\boldsymbol{x}}_{k+1|k}$, propagating it afterwards using $\boldsymbol{C}$. At this point, the estimate covariance is also determined:

$$\boldsymbol{P}_{k+1|k} = \boldsymbol{F}_k\boldsymbol{P}_{k|k}\boldsymbol{F}_k^T + \boldsymbol{Q}_k, \quad \boldsymbol{F}_k = \left.\frac{\partial f}{\partial \boldsymbol{x}}\right|_{\hat{\boldsymbol{x}}_{k|k}, u_k} \quad (21)$$

with $\boldsymbol{F}_k$ being the Jacobian of f around the current estimate.

Then, the Kalman gain, which represents the weight placed on the measurement relative to the process dynamics prediction in the state estimate update stage, can be computed:

$$\boldsymbol{K}_{k+1} = \boldsymbol{P}_{k+1|k}\boldsymbol{C}^T(\boldsymbol{C}\boldsymbol{P}_{k+1|k}\boldsymbol{C}^T + \boldsymbol{R}_k)^{-1} \quad (22)$$

The Kalman gain allows for the state estimates and its covariance to be updated, based on a comparison between the measurement, $\boldsymbol{y}_{k+1}$, and the filter prediction:

$$\begin{aligned} \hat{\boldsymbol{x}}_{k+1|k+1} &= \hat{\boldsymbol{x}}_{k+1|k} + \boldsymbol{K}_{k+1}(\boldsymbol{y}_{k+1} - \boldsymbol{C}\hat{\boldsymbol{x}}_{k+1|k}), \\ \boldsymbol{P}_{k+1|k+1} &= (\boldsymbol{I} - \boldsymbol{K}_{k+1}\boldsymbol{C})\boldsymbol{P}_{k+1|k} \end{aligned} \quad (23)$$

where $\boldsymbol{I}$ is the appropriate dimension identity matrix. Since the sensors were not modelled in this work, the measurement comes directly from the model of the system.

Considering the aforementioned, the EKF takes as inputs the vertical position, the vertical velocity and the total thrust force (needed to update the states according to equation 14) of the system and estimates the new dynamics, including Θ. After that, a controller, based on the gain-scheduling approach, uses the instantaneous value of Θ to linearize the simplified model around the new operating point and compute an appropriate LQR gain, $\boldsymbol{K_m}(\Theta_k)$. This controller also adapts the trim input according to the new mass of the system.

$$\begin{aligned} u_{0,k} &= m_k g = \frac{m_f}{\Theta_k} g, \\ u_k &= u_{0,k} - \boldsymbol{K_m}(\Theta_k)(\hat{\boldsymbol{x}}_k - \boldsymbol{x}_{k_{ref}}) \end{aligned} \quad (24)$$

with $\boldsymbol{x}_{k_{ref}}$ describing the vertical position reference.

5.3. MRAC - Lyapunov Method

MRAC is an adaptive control scheme in which the basic principle is to build a reference model that specifies the desired performance of the controller. Then an adjustment mechanism compares the system output with that of the reference model and adapts the controllers parameters so that the error is driven to zero [17].

In this work, the MRAC scheme is designed following the Lyapunov method. This method uses Lyapunov's stability theory to determine the adjustment law while ensuring the stability of the control system. As such, Lyapunov design consists in finding a Lyapunov function, $V(x,t)$, with continuous partial derivatives, that is positive definite and the derivative of which is negative (semi-)definite [18]. This function is chosen as depending on the controller parameters and the parameter adjustment law is determined in such a way that the second condition is satisfied. Here, the MRAC controller was designed as having only one adjustable parameter, ϑ.

The dynamics of the simplified model is described by equation 14 and can be written in state-space formulation as equation 19, with a variable mass m instead of m_f. Since the aim is for the controller to be able to control the vertical dynamics of the system in the presence of variable mass properties, the reference model was defined as:

$$\begin{aligned} &\dot{\boldsymbol{x}}_{\boldsymbol{m}} = \boldsymbol{A_m}\boldsymbol{x_m} + \boldsymbol{B_m}\boldsymbol{x_r}, \quad with \\ &\boldsymbol{A_m} = \begin{bmatrix} 0 & 0 \\ 1 & 0 \end{bmatrix} - \begin{bmatrix} \frac{1}{m_f} \\ 0 \end{bmatrix} \boldsymbol{K_m} \quad and \quad \boldsymbol{B_m} = \begin{bmatrix} \frac{1}{m_f} \\ 0 \end{bmatrix} \boldsymbol{K_m} \end{aligned} \quad (25)$$

In this equation, $\boldsymbol{x_r}$ is a vector that specifies the reference altitude for the system and $\boldsymbol{K_m}$ is the LQR gain of equation 24 for $\Theta = 1$, which means $m = m_f$. Thus, the reference model describes the simplified model dynamics stabilized for a constant mass.

After, the control law was defined, with the adjustable parameter ϑ adapting the inner loop controller. This law is given by:

$$u = \vartheta u_c, \quad with \quad u_c = \boldsymbol{K_m}(\boldsymbol{x} - \boldsymbol{x_r}) \quad (26)$$

Here, u_c is the inner loop control signal that stabilizes the system for a constant mass. Then, ϑ adjusts this signal to the variable dynamics of the system. Considering this, the closed loop state equation takes the form:

$$\begin{aligned} \dot{\boldsymbol{x}} &= (\boldsymbol{A} - \vartheta \boldsymbol{B}\boldsymbol{K_m})\boldsymbol{x} + \vartheta \boldsymbol{B}\boldsymbol{K_m}\boldsymbol{x_r} \\ &= \boldsymbol{A_c}(\vartheta)\boldsymbol{x} + \boldsymbol{B_c}(\vartheta)\boldsymbol{x_r} \end{aligned} \quad (27)$$

where $\boldsymbol{A_c}(\vartheta)$ and $\boldsymbol{B_c}(\vartheta)$ are the closed loop matrices depending on the parameter ϑ. The system output follows exactly the reference model output if there is a parameter value, ϑ_0, for which the following relation holds [19], [20]:

$$\boldsymbol{A_c}(\vartheta_0) = \boldsymbol{A_m}, \quad \boldsymbol{B_c}(\vartheta_0) = \boldsymbol{B_m} \quad (28)$$

In order to minimize the error between the system behaviour and that of the reference model, defined here as $\boldsymbol{e} = \boldsymbol{x} - \boldsymbol{x_m}$, the error equation was derived:

$$\begin{aligned} \dot{\boldsymbol{e}} &= \dot{\boldsymbol{x}} - \dot{\boldsymbol{x}}_{\boldsymbol{m}} = \boldsymbol{A}\boldsymbol{x} + \boldsymbol{B}u - \boldsymbol{A_m}\boldsymbol{x_m} - \boldsymbol{B_m}\boldsymbol{x_r} \\ &= \boldsymbol{A_m}\boldsymbol{e} + (\boldsymbol{A} - \vartheta \boldsymbol{B}\boldsymbol{K_m} - \boldsymbol{A_m})\boldsymbol{x} + (\vartheta \boldsymbol{B}\boldsymbol{K_m} - \boldsymbol{B_m})\boldsymbol{x_r} \\ &= \boldsymbol{A_m}\boldsymbol{e} + \boldsymbol{\Psi}(\vartheta - \vartheta_0) \end{aligned} \quad (29)$$

Finally, a Lyapunov function was chosen so that the adjustment law could be defined [18]:

$$V(e,\vartheta) = \frac{1}{2}(\gamma \boldsymbol{e}^T \boldsymbol{P}\boldsymbol{e} + (\vartheta - \vartheta_0)^2) \tag{30}$$

where γ is the adaptation gain of the controller and $\boldsymbol{P}$ is a positive definite matrix that is the solution of the Riccati equation for gain $\boldsymbol{K_m}$. Therefore, the derivative of this function is given by:

$$\begin{aligned}\dot{V}(\boldsymbol{e},\vartheta) &= \frac{\gamma}{2}(\dot{\boldsymbol{e}}^T \boldsymbol{P}\boldsymbol{e} + \boldsymbol{e}^T \boldsymbol{P}\dot{\boldsymbol{e}}) + (\vartheta - \vartheta_0)\dot{\vartheta} \\ &= -\frac{\gamma}{2}\boldsymbol{e}^T \hat{\boldsymbol{Q}}\boldsymbol{e} + (\vartheta - \vartheta_0)(\dot{\vartheta} + \gamma \boldsymbol{\Psi}^T \boldsymbol{P}\boldsymbol{e})\end{aligned} \tag{31}$$

where the last equality uses the result of equation 29 and comes from the application of the Lyapunov equation to matrix $\boldsymbol{A_m}$. This equation is given by $\boldsymbol{A}^T\boldsymbol{P} + \boldsymbol{P}\boldsymbol{A} = -\hat{\boldsymbol{Q}}$ and Lyapunov's stability theory states that, as long as $\boldsymbol{A}$ is stable, and $\boldsymbol{P}$ is a positive definite symmetric matrix, $\hat{\boldsymbol{Q}}$ is also positive definite and symmetric [18]. To obtain a negative definite derivative of V, the adjustment law for ϑ was chosen as:

$$\dot{\vartheta} = -\gamma \boldsymbol{\Psi}^T \boldsymbol{P}\boldsymbol{e} \tag{32}$$

which results in $\dot{V} = -\frac{\gamma}{2}\boldsymbol{e}^T \hat{\boldsymbol{Q}}\boldsymbol{e}$, confirming the function's negative definiteness.

6. Simulation Results

In this section, the final controllers implemented on the octorotor model are presented and their performances are discussed, based on the simulations carried out.

6.1. LQR Controller with EKF and Trim Input Adaptation

The first control system implemented makes use of the 12 states LQR controller to stabilize the attitude of the octorotor and control its translational motion, through the feedback law of equation 18. Then, to adapt the system to the variable mass properties, the adaptive controller adjusts the trim input vector $\boldsymbol{\Delta}_0$.

The adaptive controller of equation 24, implemented on the simplified model, was adjusted to the octorotor control system as a trim input adaptation mechanism. Instead of determining a new gain depending on the instantaneous mass of the system, the control is totally carried out by the 12 states LQR, and the EKF estimates of Θ are used to compute the new equilibrium thrust force, $F_0(k) = m_k g$, with $m_k = \frac{m_f}{\Theta_k}$. After that, using the actuation dynamics, this force is used to determine the vector $\boldsymbol{\Delta}_0(k)$. The block diagram of this controller is shown in figure 6.

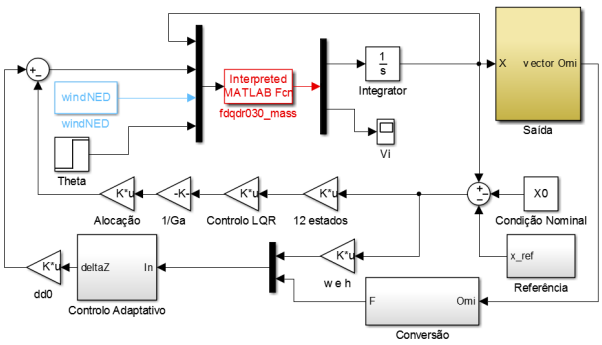

Figure 6: LQR controller with EKF and trim input adaptation

To test the performance of this controller, a simulation was carried out where the octorotor is initially at rest, with $\Theta = \Theta_i$, $\boldsymbol{r_G} = \boldsymbol{r_{G_i}}$ and $\boldsymbol{J_G} = \boldsymbol{J_{G_i}}$. Then, a reference input vector is set to $\boldsymbol{x}_{ref} = [0\ 0\ 0\ 0\ 0\ 0\ 1\ 2\ -1\ 0\ 0\ 0]$ and, after the system stabilizes in the reference position, a step mass reduction of 10% is introduced. The results are shown in figures 7 and 8.

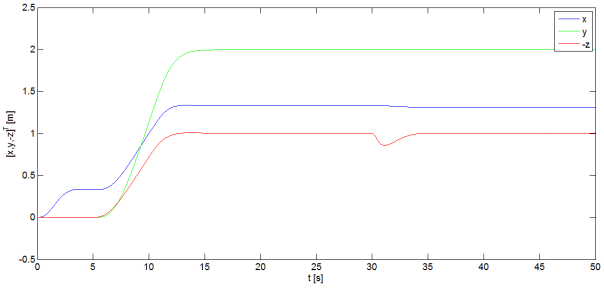

Figure 7: Position control with variable mass (EKF)

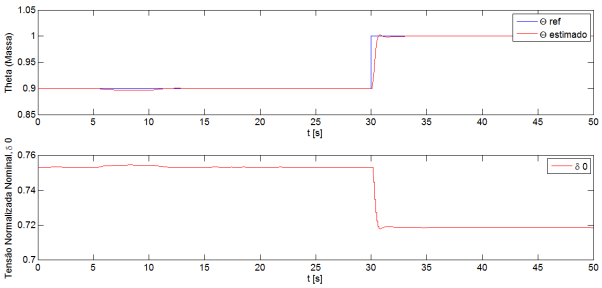

Figure 8: Estimation of Θ and trim input variation

As it can be seen in figure 7, the control system stabilizes the position of the octorotor according to the reference input. The mass variation introduced causes an altitude loss of approximately $14cm$, from which the system recovers in less than $5s$. The longitudinal position, x, presents a static error of about $30cm$ due to the offset in the position of the center

of gravity. In figure 8 it can be seen that the EKF estimates Θ correctly. As such, the trim input is adjusted accordingly.

6.2. LQR Controller with Lyapunov-based MRAC

In this control system, the LQR is used to stabilize the attitude of the octorotor and control its horizontal motion. As such, the first row of matrix $\boldsymbol{K_{LQR}}$, corresponding to the altitude control action, was suppressed. The MRAC controller was then introduced as an altitude control loop. Since the simplified model represents the vertical dynamics of the octorotor, there was no need to perform significant changes in the controller. The main difference is that the MRAC control signal, which is a force, is converted to an appropriate control input using the actuation dynamics and added to the control signal vector coming from the LQR, before applying it to matrix $\boldsymbol{M}^{+}$. The block diagram of this control system is shown in figure 9.

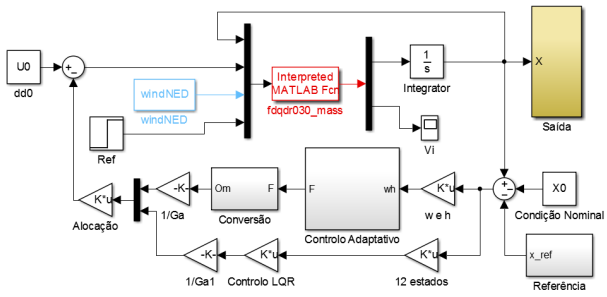

Figure 9: LQR controller with Lyapunov-based MRAC

The performance of the controller was tested using the same simulation conditions as before. The results are presented in figures 10 and 11.

In figure 10 it can be seen that in the horizontal position control, the performance of the control system is the same as in the previous case, since this part is carried out by the LQR controller. With respect to the altitude control, the mass loss does not have an impact as significant as before, mainly because the adjustment mechanism starts acting as soon as the altitude error appears. As such, the altitude loss is about $2cm$. On the other hand, as shown in figure 11, the MRAC controller is not able to drive the error to zero in the simulation time frame, because the adjustment is more gradual. Nevertheless, the error is less than $1cm$ and can therefore be neglected. In figure 11 it is also shown the evolution of the normalized voltages for each motor, that are changed to compensate for the mass loss.

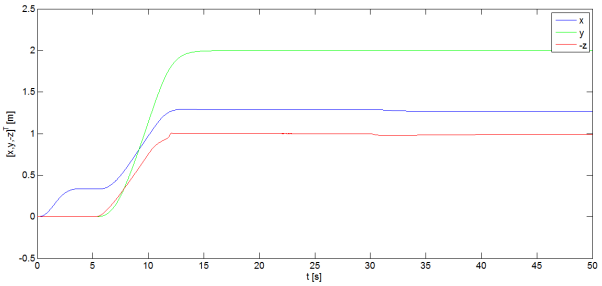

Figure 10: Position control with variable mass (MRAC)

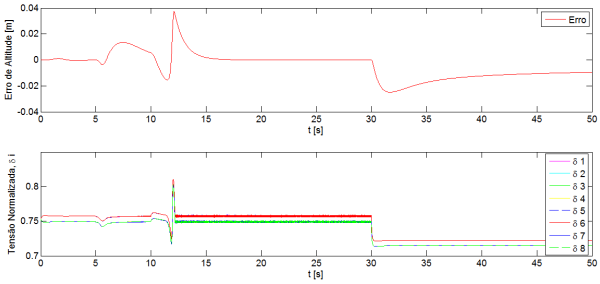

Figure 11: Altitude error and normalized voltages variations

7. Conclusions

The aim of this thesis was to design an autonomous multirotor that was capable of performing the application or removal of organic coatings in the aeronautical industry, and to develop and compare two adaptive control strategies that would allow the system to deal with disturbances in its mass properties.

With regard to the platform design, its components were selected based on initial requisites defined by a reference mission. In order for this to be a fully autonomous system, it has to be able to carry all the painting equipment, the dimensions and weights of which are very significant. This implies the acquisition of expensive components for the multirotor and even so, low flight times are achieved.

The octorotor dynamics was modelled without the usual assumptions on the center of gravity position and the inertia tensor. The implemented control strategies were able to stabilize the octorotor in these conditions and with variations in its mass. It was concluded that the adaptive controller that used the EKF to estimate the mass and then adapt the trim input produced a faster response to the mass variations, but was more significantly affected by it, when compared with the Lyapunov-based MRAC.

From the work presented here, some developments can be made. For example, it would be important to search for more accurate position sensors for the platform than the ones considered in this

work, since this is a very meticulous task that requires extremely accurate positioning. Besides that, this sensors should be modelled in order to make a more realistic model of the octorotor. It would also be useful to construct a platform prototype, in order to test different control systems in real flight. Another important improvement would be the development of control systems that would be able to adapt the entire octorotor dynamics to this kind of mass and inertia disturbances. Finally, it would be interesting to study the economic viability of this concept and its impact on the industry.

Acknowledgements

I would like to thank my supervisors, Professor Filipe Cunha and Professor José Raúl Azinheira for all the help and guidance provided and most of all, for their much appreciated patience since the beginning of this work.

I would also like to thank my family and my close friends for their unconditional support. Without them this would have never been possible.

Finally, I would like to express my gratitude to Instituto Superior Técnico and all the Professors with whom I have studied, for helping me grow both intellectually and as a person.

References

[1] Umberto Morelli. Preliminary Design of an Aircraft Automatic Painting and Paint Removal System. Master's thesis, Instituto Superior Técnico, 2016.

[2] United States Air Force. *Application and Removal of Organic Coatings , Aerospace and Non-Aerospace Equipment - TO 1-1-8 Technical Manual*, 2016.

[3] Lockheed Martin. *C-130J Super Hercules - Specification Book.*

[4] FAA. Aircraft Painting and Finishing. In *Aviation Maintenance Technician HandbookAirframe Volume 1.* 2012.

[5] GRACO Training. *Air Spray Techniques - Videotape Summary.*

[6] International Marine Coatings. *Marine Paint Guide - Theoretical & Practical Coverage*, 2004.

[7] European Parliment. Directive 97/23/EC of the European Parliment and of the Council of the European Union. 110:1–74, 2013.

[8] Samir Bouabdallah. Design and Control of Quadrotors with Application to Autonomous Flying. Master's thesis, École Polytechnique Fédérale de Lausanne, 2007.

[9] José Raúl Azinheira and Alexandra Moutinho. Modelação e Controlo de Drones Multirotores - Simulação e Projecto em MATLAB/Simulink, 2016.

[10] Jorge Miguel Brito Domingues. Quadrotor prototype. Master's thesis, Instituto Superior Técnico, 2009.

[11] Rikky R. P. R. Duivenvoorden. Quadrotor Control in the Presence of Unknown Mass Properties. Master's thesis, University of Toronto, 2016.

[12] Ferdinand P. Beer and E. Russel Johnston. *Vector Mechanics for Engineers: Statics.* McGraw-Hill, New York, 5nd edition edition, 1997.

[13] J. Gordon Leishman. *Principles of Helicopter Aerodynamics.* Cambridge University Press, New York, 2nd edition edition, 2006.

[14] Stephen Boyd and Craig Barratt. *Linear Controller Design: Limits of Performance.* Prentice-Hall, 1991.

[15] Guillaume J J Ducard and Minh-Duc Hua. Discussion and Practical Aspects on Control Allocation for a Multi-Rotor Helicopter. In *International Conference on Unmanned Aerial Vehicle in Geomatics*, volume XXXVIII, pages 1–6, Zurich, Switzerland, 2011.

[16] Mohinder S. Grewal and Angus P. Andrews. *Kalman Filtering: Theroy and Practice Using MATLAB.* Wiley, 3rd edition edition, 2008.

[17] Swarnkar Pankaj, Shailendra Jain, and Nema R. K. Comparative Analysis of MIT Rule and Lyapunov Rule in Model Reference Adaptive Control Scheme. *Innovative Systems Design and Engineering*, 2(4):154–163, 2011.

[18] Guy Dumont. EECE 574 - Adaptive Control: Model-Reference Adaptive Control - An Overview, January 2013.

[19] Yuan-Rui Chen, Jie Wu, and Norbert C. Cheung. Lyapunov's Stability Theory-Based Model Reference Adaptive Control for Permanent Magnet Linear Motor Drives. In *First International Conference on Power Electronics Systems and Applications*, pages 260–266, Hong Kong, 2004. IEEE.

[20] M. P. R. V. Rao. New Design of Model Reference Adaptive Control Systems. *Journal of Applied Mechanical Engineering*, 3(1):3–5, 2014.